IEEE Access
Multidisciplinary : Rapid Review : Open Access Journal

Received 30 December 2023, accepted 14 February 2024, date of publication 5 March 2024, date of current version 13 March 2024.

Digital Object Identifier 10.1109/ACCESS.2024.3373790

RESEARCH ARTICLE

Analytical Modeling of Depletion-Mode MOSHEMT Device for High-Temperature Applications

NAEEMUL ISLAM[1], MOHAMED FAUZI PACKEER MOHAMED[1], NORHAWATI AHMAD[2,3], (Member, IEEE), MUAMMAR MOHAMAD ISA[2,3], (Member, IEEE), ALHAN FARHANAH ABD RAHIM[4], AND KHALED AHMEDA[5]

[1]School of Electrical and Electronic Engineering, Engineering Campus, Universiti Sains Malaysia, Nibong Tebal, Pulau Pinang 14300, Malaysia
[2]Faculty of Electronic Engineering and Technology, Universiti Malaysia Perlis, Arau, Perlis 02600, Malaysia
[3]Centre of Excellence for Micro System Technology (MiCTEC), Universiti Malaysia Perlis, Arau, Perlis 02600, Malaysia
[4]Faculty of Electrical Engineering, Universiti Teknologi MARA, Cawangan Pulau Pinang, Permatang Pauh, Pulau Pinang 13500, Malaysia
[5]Research and Development Center, Dynex Semiconductor Ltd., Lincoln, LN6 3LF England, U.K.

Corresponding authors: Mohamed Fauzi Packeer Mohamed (fauzi.packeer@usm.my) and Norhawati Ahmad (norhawati@unimap.edu.my)

This work was supported by the Ministry of Higher Education Malaysia for funding through the Fundamental Research Grant Scheme (FRGS) under Grant FRGS/1/2018/TK08/UNIMAP/02/1, and by Universiti Sains Malaysia Research University Incentive (RUI) under Grant 1001/PELECT/8014134.

ABSTRACT An analytical model for depletion-mode MOSHEMTs for high-temperature applications is compared against the experimental GaN HEMT data of the AlGaN/GaN MOSHEMT for temperature dependence of 2DEG simulated at 75 °C and 125 °C. Both temperatures reduce the 2DEG density by 4 % in the GaN HEMT and 3 % in the AlGaN/GaN MOSHEMT. The cause of this diminishing effect is determined to be the decrease of the conduction band offset at high temperatures. Additionally, the device performance degrades at high temperatures due to the immature behaviour of GaN material when it operates at high-power dissipation with poor thermal conductivity. The simulated AlGaN/GaN MOSHEMT performance is comparatively improved compared to the experimental AlGaN/GaN HEMT devices. This improvement could be used to understand the nature of the 2DEG density vs the temperature, hence could enhance the experimental performance of the AlGaN/GaN MOSHEMT.

INDEX TERMS AlGaN, GaN, MOSHEMT, 2DEG, wide-bandgap, semiconductor device.

I. INTRODUCTION

Over the past ten years, gallium nitride (GaN), which has excellent performance characteristics including a wide band gap, high breakdown field, high electron mobility, high saturation velocity, low noise, and low thermal impedance, has become a popular material for fabricating semiconductor devices [1], [2], [3]. Thus, several market-driven industries, such as high-frequency communication, RF power devices, high-power conversion, photonics, and control, have reported the use of GaN-based devices [4], [5].

The associate editor coordinating the review of this manuscript and approving it for publication was Francesco G. Della Corte.

The high electron density at the AlGaN/GaN interface is one of the characteristics of the AlGaN/GaN heterostructure that makes it suitable for high-power applications. Due to spontaneous and piezoelectric polarization-induced charges at the AlGaN surface, the AlGaN/GaN interface, and the GaN/substrate interfaces, GaN-based epitaxial layers grown in the wurtzite crystal structure exhibit distinctive material characteristics such as built-in electric fields. Therefore, a positive sheet charge must be present at the AlGaN surface in order for the 2DEG to develop at the AlGaN/GaN interface [6], [7]. However, for high-power, high-frequency, and high-temperature applications with minimal gate leakage current, AlGaN/GaN metal oxide semiconductor high electron mobility transistors (MOSHEMTs) are very fascinating [8].

© 2024 The Authors. This work is licensed under a Creative Commons Attribution 4.0 License.
For more information, see https://creativecommons.org/licenses/by/4.0/

Due to the low cost and the large size of the silicon substrate, the GaN devices on the silicon substrate help to solve the substrate's cost and heat sink capability [9].

Nevertheless, GaN technology has been constrained by a few undesirable scattering phenomena. The trapping effect has been measured and characterized [10] and simulated at higher frequency applications [11]. High leakage currents occur triggered by scattering phenomena like dislocation scattering, charged impurity scattering, roughness scattering at the interface, and phonon scattering [12], [13], [14], consequently affecting the sheet carrier density and 2DEG of GaN HEMTs. Furthermore, the Schottky and Ohmic contacts degrade at higher temperatures, which reflects the importance of temperature stability and reliability for HEMTs. An analytical model for 2DEG charge density and TCAD simulation for the buffer layer to increase the breakdown critical field has been studied in [15], [16], and [17]. Therefore, it is vital to analyze how the 2DEG transport works at different temperatures because the transport characteristics of 2DEG significantly impact the device's performance. There are various simulations based on mole fractions of AlGaN/GaN and AlGaAs/GaAs HEMTs on 2DEG transport properties [18]. Wang et al. [19] investigated how the 2DEG heterostructure in $Al_{0.18}Ga_{0.82}N$/GaN is affected by high temperatures. The device modelling must include a thermal model. For example, an analytical thermal model established by Li et al. uses a conformal mapping method [20]. Alim et al. [21] described how temperature has been found to affect the DC and RF transconductance of many significant HEMT technologies. Mann et al. [22] present an ASM-HEMT that is temperature-dependent for modeling GaN HEMTs at high temperatures. Other works on nonlinear temperature-dependent modeling of GaN HEMTs include [23], [24], [25]. The impact of temperature on both the TLM structure and knee walkout in GaN HEMT devices has been thoroughly investigated in studies [26], [27], which focused on simulation analysis.

In this article, we investigated the AlGaN/GaN MOSHEMTs 2DEG transport characteristics through TCAD simulation and compared analytically with experimental data of AlGaN/GaN HEMTs at temperatures of 75 °C and 125 °C. Here, we study the behaviour of an AlGaN/GaN MOSHEMT against experimental conventional GaN HEMT to give us an insight view how its behaviour affects different GaN based devices for a high temperature application. There are some diversions in the curve because no calibration has been performed.

II. DEVICE DESIGN

The AlGaN/GaN MOSHEMT has been designed using Silvaco's Atlas TCAD device simulation software, as shown in Fig. 1. The device building is composed of a 25 nm thick $Al_{0.25}Ga_{0.75}N$ barrier layer and a 4.2 μm doped GaN buffer layer on a silicon substrate. The MOSHEMT has a doping concentration of acceptor traps of 5×10^{19} cm^{-3} in the GaN buffer layer and an n-type uniform background doping of 3×10^{16} cm^{-3}. From the top, the proper electron confinement towards the buffer is provided by the $Al_{0.25}Ga_{0.75}N$ barrier layer. Due to piezoelectric and spontaneous polarization effects, numerous electrons spontaneously emerge at the GaN channel without intentional doping, producing a 2DEG [6], as displayed in Fig. 2, while Al_2O_3 is used as the gate dielectric where thickness, permittivity, and bandgap are 10 nm, 9 and 7 eV, respectively [28].

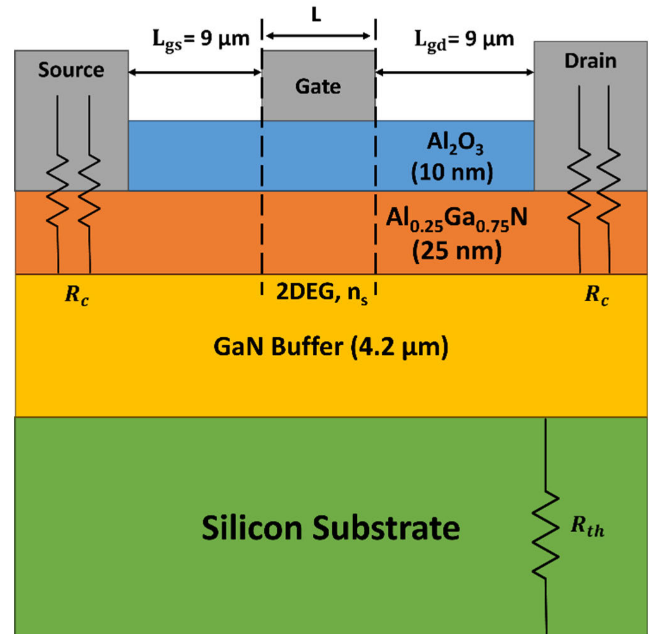

FIGURE 1. Schematic cross section of the simulated AlGaN/GaN MOSHEMT with Silicon substrate.

Furthermore, the gate length of the device is 10 μm, with a work function of 4.7 eV. The gate electrode is assumed to be made of metal. The distance between the gate to the source and to the drain is 9 μm. As for simulations, we incorporated models such as the Fermi-Dirac model in order to use Fermi statistics; the Shockley-Read-Hall model is used for carrier generation and recombination; *Fnord*, a statement of the *Albrct* to take into account Albert's mobility model and saturation velocity; a model of Joule heat for heat generation effect; a statement *Gansat* which is nitride-specific mobility model; and the epitaxial strain model caused by a lattice mismatch and a spontaneous polarization, calculated strain and polarization are evoked. The Block method was selected to solve linearized equations in the Atlas TCAD [29].

III. DEVICE DESCRIPTION

Fig. 2 presents the calculated polarization charge densities at the $Al_2O_3/Al_{0.25}Ga_{0.75}N$, $Al_{0.25}Ga_{0.75}N$/GaN, and GaN/substrate interfaces that calculation is done by Python software where the equations (1) to (10) used. Hence, spontaneous polarization (P_{sp}) presented in the equation (1) [30], [31] is given by:

$$P_{sp}(x) = (-0.052x - 0.029)\, C/m^2 \quad (1)$$

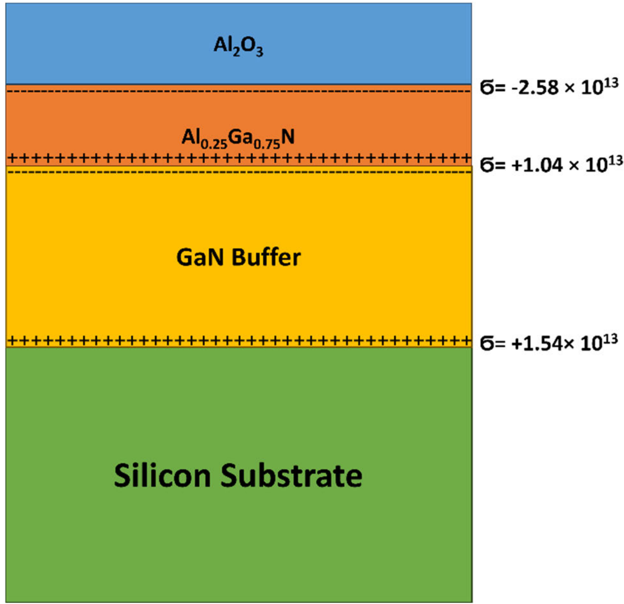

FIGURE 2. Calculated polarization-induced sheet charge densities at Al_2O_3/AlGaN, AlGaN/GaN, and GaN/substrate interface.

Alternatively, for a precise interpolation, a bowing parameter b can be used:

$$P_{sp}(x) = (xP_{sp}(AlN) + (1-x)P_{sp}(GaN) + bx(1-x)) \tag{2}$$

While the lattice constant (a_0 and c_0) for $Al_xGa_{1-x}N$ are expressed in the equations (3) and (4), where x = Al mole fraction.

$$a_0(x) = (-0.077x + 3.189) \times 10^{-10}m \tag{3}$$

$$c_0(x) = (-0.203x + 5.189) \times 10^{-10}m \tag{4}$$

Furthermore, the elastic constants (c_{13} and c_{33}) can be written as in equations. (5) and (6) [30], [31].

$$c_{13}(x) = (5x + 103)\,GPa \tag{5}$$

$$c_{33}(x) = (-32x + 405)\,GPa \tag{6}$$

The magnitude of the polarization-induced sheet charge (σ) at the AlGaN/GaN interface can be calculated using equations (7) and (8).

$$|\sigma(x)| = |P_{PE}(Al_xGa_{1-x}N) + P_{SP}(Al_xGa_{1-x}N) - P_{SP}(GaN)| \tag{7}$$

$$|\sigma(x)| = |2\frac{a(0) - a(x)}{a(x)}\left\{e_{31}(x) - e_{33}(x)\frac{c_{13}(x)}{c_{33}(x)}\right\} + P_{SP}(x) - P_{SP}(0)| \tag{8}$$

where e_{13} *and* e_{33} are piezoelectric constants as shown in the equations (9) and (10) [30], [31].

$$e_{13}(x) = (-0.11x - 0.49)\,C/m^2 \tag{9}$$

$$e_{33}(x) = (0.73x + 0.73)\,C/m^2 \tag{10}$$

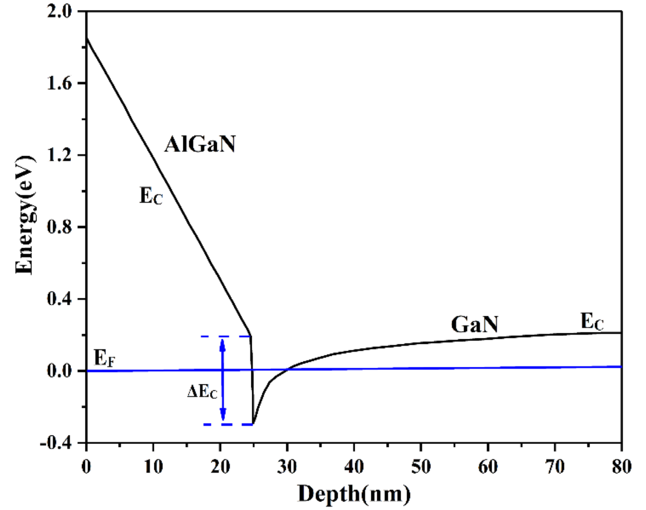

FIGURE 3. Conduction energy band diagram of AlGaN/GaN MOSHEMT device at 25 °C temperature.

A. TRANSPORT FEATURES OF 2DEG

The band diagram in Fig. 3 is obtained after simulating the Fig. 1 structure. The conduction band E_c crosses the Fermi level with an energy of −0.303 eV at a depth of 25 nm from the Schottky gate contact, where the two-dimensional electron gas (2DEG) is formed at the $Al_{0.25}Ga_{0.75}N$/GaN interface. The coupled Schrödinger and Poisson equations could be solved to determine the 2DEG density for $Al_{0.25}Ga_{0.75}N$/GaN heterostructures. The electrostatic potential is correlated to charge distribution by Poisson's equation, as shown in equation (11) [32].

$$\frac{d}{dz}\left(\varepsilon\frac{d}{dz}V(z)\right) = q\left(N_D^+ - N_E\right) \tag{11}$$

The density of ionized donors denotes N_D^+, whereas the density of conduction electrons expressed by N_E. Schrodinger's equation illustrates the wave function of the ith sub-band ψ_i for free electrons [33].

$$\left[-\frac{h^2}{2m^*}\frac{d^2}{dz^2} + [V(z)]\right]\psi_i(z) = E_i\psi_i(z) \tag{12}$$

The electron effective mass defines m^* and the Eigen-energy of the ith sub-band ψ_i is represented by E_i [33]. Thus, equation (12) can be presented as equation (13). Furthermore, by solving H (Hamiltonian operator):

$$H\psi_i(z) = E_i\psi_i(z) \tag{13}$$

can be written as:

$$(H - I\lambda)\,\psi_i(z) = 0 \tag{14}$$

Equation (12) Eigenvalue for the Eigen energy E_i is indicated by λ. ψ_i may have an unlimited number of dependent solutions due to $|H - I\lambda|\,\psi_i = 0$, as presented by R. M. Chu [32]. Now, the 2DEG, $n_{2D}(z)$ is provided by the

equation (15).

$$n_{2D}(z) = \sum_i N_i |\psi_i(z)|^2 \tag{15}$$

where N_i is the per unit area electrons for the E_i the energy state of ψ_i wave function.

Hence, the density of states (DOS) integration function, Fermi-Dirac probability function with $g(E), f(E)$ denotes N_i as given in the equation (16). Here, $(E) = {m^*}/{\pi h^2}$, so the equation (16).

$$N_i = \int_{E_i}^{\infty} g(E) f(E)\, dE \tag{16}$$

can be written as:

$$N_i = {m^*}/{\pi h^2} \int_{E_i}^{\infty} \frac{1}{1 + exp\left(\frac{E_i - E_F}{kT}\right)} dE \tag{17}$$

simplified to the equation:

$$N_i = {m^* kT}/{\pi h^2} In\left[1 + exp\left(\frac{E_F - E_i}{kT}\right)\right] \tag{18}$$

The temperature, the Boltzmann constant, and the Fermi level are expressed by T, k, and E_F respectively. Thus, under equilibrium conditions, the sub-band obeys Fermi statistics, and the equation (15) is given by,

$$n_{2D}(z) = \sum_i {m^* kT}/{\pi h^2} |\psi_i(z)|^2 In\left[1 + exp\left(\frac{E_F - E_i}{kT}\right)\right] \tag{19}$$

Equation (19) shows that the three-dimensional Fermi-Dirac statistics is used to calculate the electron concentration when the distance between successive sub-band energies gets lower than the thermal energy, kT.

B. 2DEG CHARGE DENSITY AND THRESHOLD VOLTAGE

The low electric field and a provided gate bias, the 2DEG sheet carrier density [34], n_s can be presented as an equation (20).

$$n_s = \frac{\varepsilon}{qd_{AlGaN}}\left(V_{gs} - V_{th}\right) \tag{20}$$

Here , V_{th} is the threshold voltage, and a gate voltage denoted as V_{gs} and d_{AlGaN} is the AlGaN barrier thickness, and $\frac{\varepsilon}{d_{AlGaN}} = C_n$, C_n is the gate capacitance. Considering the various band discontinuities, the sum of gate capacitance with two contributions: $C_n^{-1} = C_{Al2O3}^{-1} + C_{barrier}^{-1}$, having gate dielectric and the AlGaN barrier. Hence, the threshold voltage with the polarization-induced charge is calculated analytically by equation (21) [34].

$$V_{th} = \phi_b - \Delta E_c - qC_n^{-1} P_{total} \tag{21}$$

where the total polarization charge is expressed by P_{total}, the conduction band offset in the AlGaN/GaN heterostructure defined by ΔE_c, and the Schottky barrier height denotes ϕ_b.It is noticed that after the solution of the Schrodinger and Poisons equation [30], [35], the 2DEG sheet carrier density is written as in equation (22).

$$n_s = \frac{\varepsilon}{qd_{AlGaN}}\left(V_{gs} - V_{th} - \frac{E_F(n_s)}{q}\right) \tag{22}$$

here, E_F is a function of n_s, as proposed by equation (23).

$$E_F = K_1 + K_2\sqrt{n_s} + K_3 n_s \tag{23}$$

where K_1, K_2, and K_3 indicate three dependent temperature parameters fixed numerically [36]. It can be illustrated by performing some algebra of $n_s(E_F)$, that n_s can still be described as an analytical function of the gate voltage as shown in equation (24), where $\Gamma = \left(K_3 + qC_n^{-1}\right)$. Consequently, 2DEG sheet carrier density, n_s and threshold voltage, V_{th} can be regarded as weakly temperature dependent because the polarization field is a weak function of the temperature [36].

$$n_s = \frac{1}{4\Gamma^2}\left[-K_2 + \sqrt{K_2^2 + 4\Gamma(V_{gs} - V_{th} - K_1)}\right]^2 \tag{24}$$

C. DRAIN CURRENT AND TRANSCONDUCTANCE

The ideal HEMT drain current can be derived over the channel length as provided by equation (25) or equation (26) [35], [36]. Here, the concentration of electron sheet carrier density denotes n_S, the electron charge represents q, and the channel width denotes W.

$$I_{ds}(x) = qn_S(x)Wv(x) \tag{25}$$

or

$$I_{ds}(LK_1V_{ds}) = -q\mu W \int_{V_S}^{V_D} n_S dV \tag{26}$$

Furthermore, the drift velocity with a channel, i.e., v can be expressed by equation (27). Where, in the 2DEG channel, the electron mobility denotes μ, $K_1 = {\alpha}/{E_c}$, the adjustable parameter indicates α, and the electrical critical field denotes E_c.

$$v(x) = \frac{\mu E(x)}{1 + \alpha {E(x)}/{E_c}} = \frac{\mu \frac{dV}{dx}}{1 + K_1 \frac{dV}{dx}} \tag{27}$$

Additionally, after combining equations (25) and (27) and then integrating between the limits 0 < x < L, where L is the gate length, the drain current can be written as equation (28),

$$I_{ds}\left(1 + \frac{V_{ds}}{LE_c}\right) = \mu C_n \frac{W}{L}\left(\left(V_{gs} - V_{th}\right)V_{ds} - \frac{V_{ds}^2}{2}\right) \tag{28}$$

After considering the situation ${\partial I_{ds}}/{\partial V_{ds}} = 0$, the drain voltage can be expressed by equation (29).

$$V_{ds}^{sat} = \sqrt{(LE_c)^2 + 2LE_c\left(V_{gs} - V_{th}\right)} - LE_c \tag{29}$$

The drain current can be further written as equation (30) after doing several algebras [6].

$$I_{ds}^{sat} = \mu C_n \frac{2W}{L}\left(V_{gs} - V_{th}\right)^2$$

$$\times\left[1+\sqrt{\left(1+\frac{2\mu\left(V_{gs}-V_{th}\right)}{V_{Sat}^{L}}\right)}\right]^{-2} \tag{30}$$

After Shockley's design, considering with low field mobility $V_{Sat} = \mu E$, and V_{Sat} limit to infinity, the drain current equation can be simplified to equation (31) [37].

$$I_{ds}^{sat} = \mu C_n \frac{W}{2L}\left(V_{gs}-V_{th}\right)^2 \tag{31}$$

Then, with $n_s = \frac{\varepsilon}{qd_{AlGaN}}\left(V_{gs}-V_{th}\right)$ and $\mu = {C}/{n_s^{\delta}}T^{\gamma}$, equation (30) [38], where C, δ,and γ are the empirical constant for describing the dependence on the 2DEG density n_s and temperature. The mobility constants of $\gamma = 2.7$ and δ=*0.3* have been fitted to the theoretical computed μ_{2D}(2DEG) of [39], [40] with ($\hbar\omega_0 = 91.2$ MeV, $m^*/m_0 = 0.2$, $\varepsilon_s = 8.9$ and $\varepsilon_{s,\infty} = 5.35$) for $n_s = 1 \times 10^{13}$ cm^{-2} and $T = 300$ K, respectively. However, it was reported [41] that GaN optical phonon energy ($\hbar\omega_0 \sim 90$ MeV) is high compared to the energy separation of sub-bands. The energy separation between all sub-bands, except for the first and second, is very small <1 MeV, resulting in a highly inelastic nature of polar-optical scattering. This could make the total scattering rate the sum of many intersub-band and intrasub-band scattering processes when the n_s concentration is high. This would result in a depreciation of the characteristic features of a 2DEG. For this reason, the relaxation time for the scattering of electrons in this 2DEG by optical phonons would tend to be the bulk relaxation time. So, this can be finally presented by equation (32).

$$I_{ds}^{sat} = q^2\frac{CW}{2C_nLT^{\gamma}}n_s^{2-\delta} \tag{32}$$

Now, the transconductance can be expressed by derivation of equation (32) to expression in equation (33).

$$g_m^{sat} = \frac{qCW}{2LT^{\gamma}}(2-\delta)\,n_s^{1-\delta} \tag{33}$$

This equation shows that transconductance is directly related to the mobility of electrons in the 2DEG region. As temperature increases, scattering mechanisms become more pronounced, which limits the smooth movement of electrons and, therefore, reduces mobility. So, the percentage of electrons in the 2DEG region also decreased. In short, we can say that if scattering increases, it may lead to a reduction in the mobility and 2DEG density.

Furthermore, by referring to Fig 1 and using this extremely simple question, $V_{gs} - V_{th}$ for larger V_{gs}, it could be possible to make the model more accurate by considering gate-drain series resistance, self-heating, and other degradation processes. To take into account the series resistance, the saturation voltage in the definition of equation (32) can be substituted by $V_{ds} = V_{ds}^{*} - I_{ds}R_{DS}$. So, the total resistance is $R_{DS} = 2R_c + R_{gs} + R_{gd}$, where $R_{gs} = R_{sheet}(L_{gs}W)$ and $R_{gd} = R_{sheet}(L_{gd}W)$, here L_{gs} and L_{gd} are the gate-to-source and gate-to-drain spacing. On the other hand, the 2DEG channel sheet resistance $R_{sheet}^{-1} = qn_s\mu$. Hence, the modification of equation (32) can then be shown in equation (34).

$$I_{ds}^{sat} = i_0/\left(1+\Delta\right) \tag{34}$$

where

$$\Delta = \frac{qCW}{2LT^{\gamma}}R_{DS}n_s^{1-\delta}$$

D. TEMPERATURE AND SELF HEATING

The saturation region current declines due to the self-heating effect on the AlGaN/GaN device at high current density. Essentially, channel temperature is raised by self-heating to an effective temperature, T_{ef}; this temperature relies on the dissipated power, the substrate temperature (T_{sub}), and the thermal resistance (R_{th}) as shown in equation (35).

$$T_{ef} = R_{th}I_{ds}V_{ds} + T_{sub} \tag{35}$$

the R_{th} can be expressed as equation (36) [36], [42].

$$R_{th} = (\pi K)^{-1}\, In\left[{8d_{sub}}/{\pi L}\right] \tag{36}$$

Here, the thickness of the substrate indicates d_{SUB}, the substrate thermal conductivity represents K. The thermal conductivity has been studied experimentally for sapphire, silicon, GaN, and silicon carbide (SiC) substrates [42]. Additionally, the high-temperature variation impacted the bandgap energy, effective carrier concentrations, and mobility. Thus, the bandgap energy reduces at a higher temperature, which is described by the equation (37) [43].

$$E_g = E_0 - {\alpha T^2}/{(\beta + T)} \tag{37}$$

Here, bandgap energy at *0 K* presents E_0, the empirical constants for GaN denote α and β. However, the change of temperature has not impacted on piezoelectric and spontaneous polarization coefficients [44]. Moreover, the rising temperature often causes a reduction in thermal conductivity (K), mobility (μ), and carrier concentration (n_s). By using power law, thermal conductivity is modelled through equation (38).

$$K\left(T_L\right) = K_{300}\left(\frac{T_L}{300K}\right)^{\alpha_k} \tag{38}$$

Here, the temperature reduction is modelled by the parameter α. At $K_{300} = 130$ W/mK; $\alpha = -0.43$ [45]. Caughey and Thomas use an equation like that to model low-field mobility [26], [45], [46], [47]. The mobilities are also analyzed using power laws to describe the temperature dependency as given in equation (39).

$$\mu\left(T_L\right) = \mu_{300}\left(\frac{T_L}{300K}\right)^{\alpha_\mu} \tag{39}$$

Similarly, equation (40) shows the effective carrier concentrations, which are also analyzed using power laws to describe the temperature dependency.

$$n_s\left(T_L\right) = n_{s.300}\left(\frac{T_L}{300K}\right)^{\alpha_n} \tag{40}$$

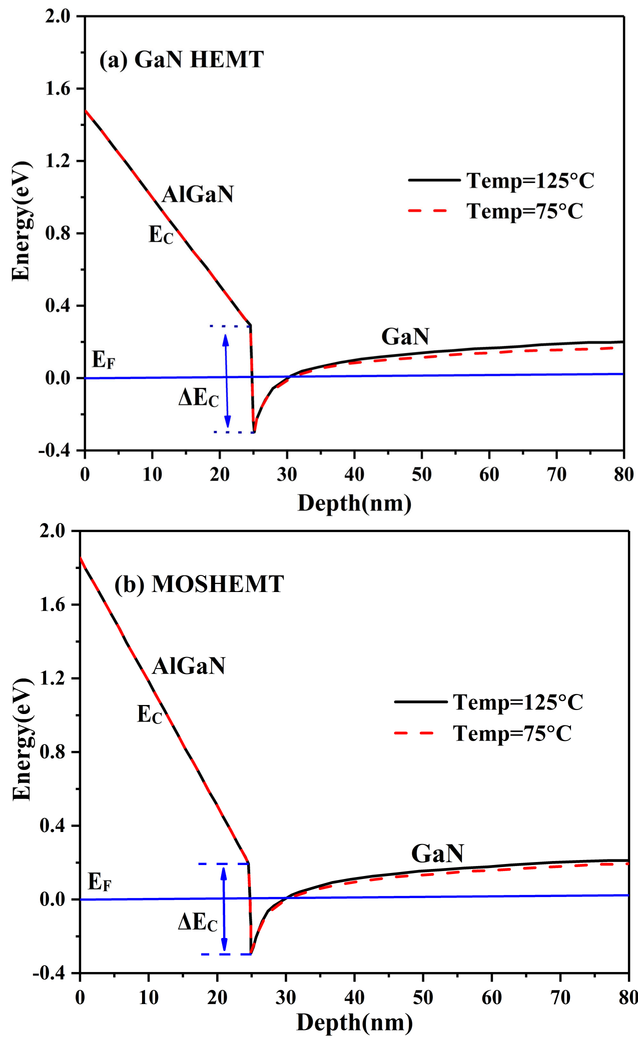

FIGURE 4. Profile of a conduction band diagram indicates that the 2DEG is reduced when the temperature is raised from 75 °C to 125 °C, changing the temperature for both (a) GaN HEMT (b) MOSHEMT.

TABLE 1. Compared data of experimental and simulational for 2DEG.

T (°C)	Experimental (eV)	Simulational (eV)
75	-0.3025	-0.220
125	-0.2985	-0.217

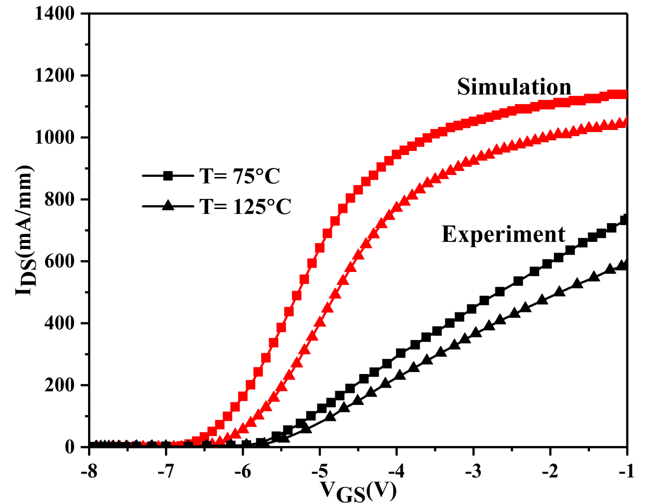

FIGURE 5. Transfer characteristics curves with different temperatures at 75 °C and 125 °C for simulation and experimental work.

IV. RESULT AND DISCUSSION

Fig. 4 shows the profile of a conduction band where the performance of 2DEG has been observed by varying the temperature. The 2DEG is reduced when the temperature is raised from 75 °C to 125 °C.

Because as the temperature increases, carriers (electrons in this case) gain more thermal energy. This increased energy can lead to greater scattering events, reducing the overall mobility of electrons in the 2DEG. Hence, conduction band energy around −0.3025 eV for 75 °C to −0.2985 for 125 °C has changed for the experimental GaN HEMT device [48]. On the contrary, the simulated MOSHEMT varied from −0.220 eV to −0.217 eV approximately. Comparing experimental and simulation data is presented in Table 1.

On the other hand, Fig 5 illustrates under the temperature variation for two particular temperature points of 75 °C and 125 °C, the simulation results of MOSHEMT show the drain-to-source current (I_{DS}) outputs for the several gates to source voltage (V_{GS}), which shows a similar behaviour of measured GaN HEMT device [48], both simulated and experimental are taken at drain voltage $V_{DS} = 15$ V.

We have observed similar performance for both simulation and experimental plots for AlGaN/GaN MOSHEMT and experimental conventional GaN HEMT; the drain to source current (I_{DS}) tends to degrade at rising temperatures due to the reduction of mobility (scattering events impede the motion of electrons) and sheet carrier concentration (Thermal energy can promote carrier generation through processes like thermal excitation or due to enhanced carrier recombination). It means GaN HEMT based devices with a different architecture for certain applications would suffer similar behaviour at high temperatures.

Moreover, at high temperatures, the threshold voltage (V_{th}) also increased in both results; for instance, the gate voltage (V_{GS}) becomes less negative when the threshold voltage (V_{th}) is moved right towards. Hence, for simulation, the V_{th} changes from around −6.9 V for 75 °C to −6.5 V for 125 °C. In the experiment case, approximately −5.42 V to −5.25 V [48], as highlighted in Table 2.

As for the 2DEG sheet carrier density, the calculated data for simulation and experimental have been demonstrated in Fig 6. It is revealed that the 2DEG sheet carrier density degrades for both devices when the temperature increases. Because at higher temperatures, various scattering mechanisms become more pronounced, such as lattice scattering, impurity scattering, and surface roughness scattering. Moreover, it induces thermal stress in the device material, potentially affecting the crystal structure and the quality of the interface between different semiconductor layers,

TABLE 2. Compared data of experimental and simulational for transfer curve.

T (°C)	Experimental (eV)	Simulational (eV)
75	-5.42	-6.9
125	-5.25	-6.5

TABLE 3. Compared data of experimental and simulation for 2DEG sheet carrier density.

T (°C)	Experimental (cm^{-2})	Simulation (cm^{-2})
75	1.12×10^{13}	1.13×10^{13}
125	1.10×10^{13}	1.11×10^{13}

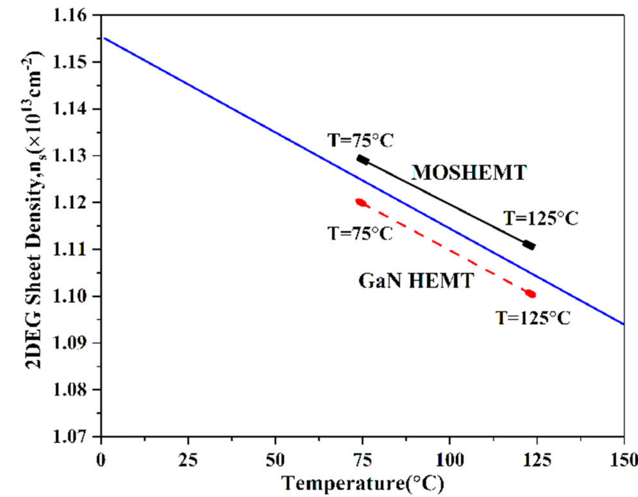

FIGURE 6. Profile of 2DEG sheet carrier density against different temperatures. This shows the 2DEG density is reduced by increasing the temperature of both devices.

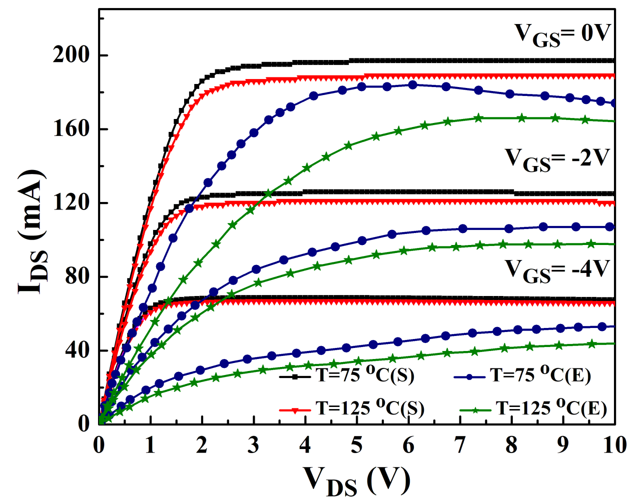

FIGURE 7. Comparison of output characteristic curves with different temperatures of MOSHEMT Vs GaN HEMT. (S = Simulation MOSHEMT, E = Experimental GaN HEMT) [49].

consequently decreasing the mobility and sheet carrier density. Thus, in the simulation MOSHEMT device, the n_s vary from 1.13×10^{13} cm^{-2} for 75 °C to 1.11×10^{13} cm^{-2} for 125 °C, whereas, for the experimental GaN HEMT device, the n_s changes from 1.12×10^{13} cm^{-2} for 75 °C to 1.10×10^{13} cm^{-2} for 125 °C [48], as represented in Table 3.

GaN HEMT [49] and simulated MOSHEMT devices in Fig. 7 show the output characteristic curves by changing the temperature at different gate bias voltages. According to Fig. 7, the drain current (I_{DS}) tends to decrease as the temperature is raised, as predicted by analytical analysis on the drain current section.GaN HEMT [49] and simulated MOSHEMT devices in Fig. 7 show the output characteristic curves by changing the temperature at different gate bias voltages. According to Fig. 7, the drain current (I_{DS}) tends to decrease as the temperature is raised, as predicted by analytical analysis on the drain current section. In the MOSHEMT simulation, for the different gate to source (V_{GS}) voltages, such as 0 V, −2 V, and −4 V, the curves demonstrate slight degradation.

On the contrary, in GaN HEMT, the experimental result indicates the temperature-dependent behaviour of I_{ds} mostly because of the degradation of carrier transport properties and the reduction in the carrier concentration in the 2DEG as a reason for carriers to experience more scattering events due to lattice vibrations and other thermal effects, at high temperatures. Besides, it can affect the subthreshold slope, which is a measure of the sensitivity of the transistor to changes in gate voltage. Therefore, a degraded subthreshold slope can result in less efficient control of the transistor, affecting the steepness of the I vs V curve.

Additionally, it is noticed that the transconductance (g_m) is degraded for both simulation and experimental devices as the temperature increases because of the reduction in mobility and sheet carrier concentration, as predicted in the analytical model on the transconductance section. Thus, it is noted that in mobility, as temperature increases, the scattering is also enhanced, which is caused by lattice vibrations and other flaws in the crystal structure.

As a result, it reduced the mobility and 2DEG density because charge carriers movement through the channel region of the device is limited by the scattering phenomena, which impacted the transconductance since it is directly related to carrier mobility. Furthermore, a soaring temperature decrease in bandgap narrows the energy gap between the Fermi level and the Conduction band. Consequently, there is a reduction in mobility. On the contrary, the rising temperature in the sheet carrier concentration generated more electron-hole pairs in the material, increasing the sheet carrier concentration. Nevertheless, this impact is frequently overshadowed by decreased mobility, and the device's total conductivity may end up declining because of this. In the simulation, g_m reduces from around 273 mS/mm to 219 mS/mm, and for the experimental, around 231 mS/mm to 167 mS/mm with the changing temperature from 50 °C to 150 °C, as illustrated in Fig 8 [48]. Furthermore, a comparison of experimental and simulation data is revealed in Table 4.

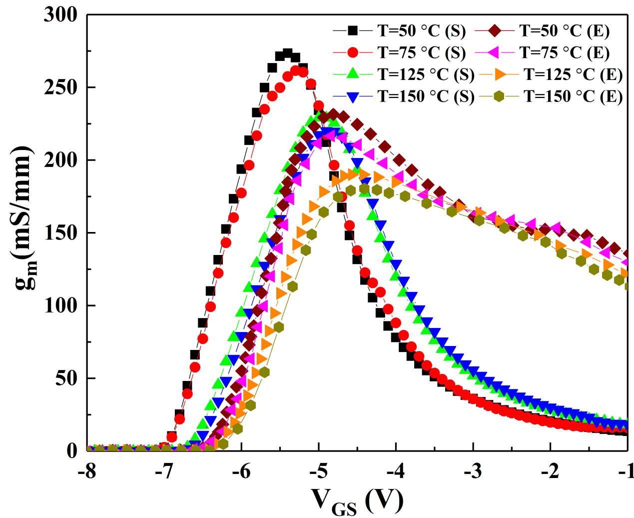

FIGURE 8. Comparison study between experimental (E) and simulation (S) behaviour of Transconductance (g_m) curves with different temperatures of 50 °C, 75 °C, 125 °C and 150 °C.

TABLE 4. Compared data of experimental and simulation for transconductance.

T (°C)	Experimental (mS/mm)	Simulation (mS/mm)
50	231	273
75	215	260
125	180	229
150	167	219

V. CONCLUSION

The primary outcome of this research is to analyze simulational and analytically the temperature dependency of 2DEG for the AlGaN/GaN MOSHEMT at temperatures of 75 °C and 125 °C. It is observed that the degradation nature of 2DEG density in both the devices. In this work, comparisons are made between the AlGaN/GaN MOSHEMT device simulated data with the experimental AlGaN/GaN HEMT device, where V_{th} improves from −6.9 V to −6.5 V for simulation and for the experimental from −5.42 V to −5.25 V, when the temperature increases from 75 °C to 125 °C. On the contrary, both devices transconductance (g_m) was reduced by roughly an average of 20 mS/mm when temperature varied systematically from from 50 °C to 150 °C. Moreover, 2DEG sheet carrier density $n_s$decreases 1.13×10^{13} cm^{-2} to 1.11×10^{13} cm^{-2} for simulated MOSHEMT and 1.12×10^{13} cm^{-2} to 1.10×10^{13} cm^{-2} for the experimental GaN HEMT.

ACKNOWLEDGMENT

The authors would like to thank USM School of Electrical and Electronic Engineering for providing research facilities, also would like to thank Prof. Karol Kalna from Swansea University for his valuable scientific discussion, and also would like to thank Universiti Teknologi MARA, Penang, for SILVACO TCAD tool support.

REFERENCES

[1] U. K. Mishra, P. Parikh, and Y.-F. Wu, "AlGaN/GaN HEMTs—An overview of device operation and applications," *Proc. IEEE*, vol. 90, no. 6, pp. 1022–1031, Jun. 2002.

[2] N. Islam, M. F. P. Mohamed, M. F. A. J. Khan, S. Falina, H. Kawarada, and M. Syamsul, "Reliability, applications and challenges of GaN HEMT technology for modern power devices: A review," *Crystals*, vol. 12, no. 11, p. 1581, Nov. 2022.

[3] A. Udabe, I. Baraia-Etxaburu, and D. G. Diez, "Gallium nitride power devices: A state of the art review," *IEEE Access*, vol. 11, pp. 48628–48650, 2023.

[4] H. Amano, "The 2018 GaN power electronics roadmap," *J. Phys. D, Appl. Phys.*, vol. 51, no. 16, Mar. 2018, Art. no. 163001.

[5] M. Meneghini, C. De Santi, I. Abid, M. Buffolo, M. Cioni, R. A. Khadar, L. Nela, N. Zagni, A. Chini, F. Medjdoub, G. Meneghesso, G. Verzellesi, E. Zanoni, and E. Matioli, "GaN-based power devices: Physics, reliability, and perspectives," *J. Appl. Phys.*, vol. 130, no. 18, Nov. 2021, Art. no. 181101.

[6] J. P. Ibbetson, P. T. Fini, K. D. Ness, S. P. DenBaars, J. S. Speck, and U. K. Mishra, "Polarization effects, surface states, and the source of electrons in AlGaN/GaN heterostructure field effect transistors," *Appl. Phys. Lett.*, vol. 77, no. 2, pp. 250–252, Jul. 2000.

[7] Y. Yusuf, M. E. A. Samsudin, M. I. M. Taib, M. A. Ahmad, M. F. P. Mohamed, H. Kawarada, S. Falina, N. Zainal, and M. Syamsul, "Two-step GaN layer growth for high-voltage lateral AlGaN/GaN HEMT," *Crystals*, vol. 13, no. 1, p. 90, Jan. 2023.

[8] X. Liu, E. K. F. Low, J. Pan, W. Liu, K. L. Teo, L.-S. Tan, and Y.-C. Yeo, "Impact of in situ vacuum anneal and SiH_4 treatment on electrical characteristics of AlGaN/GaN metal-oxide-semiconductor high-electron mobility transistors," *Appl. Phys. Lett.*, vol. 99, no. 9, Aug. 2011, Art. no. 093504.

[9] T. Uesugi and T. Kachi, "Which are the future GaN power devices for automotive applications, lateral structures or vertical structures?" in *CS Mantech Tech. Dig.*, 2011, pp. 1–4.

[10] S. J. Duffy, B. Benbakhti, W. Zhang, K. Ahmeda, K. Kalna, M. Boucherta, M. Mattalah, H. O. Chahdi, N. E. Bourzgui, and A. Soltani, "A parametric technique for trap characterization in AlGaN/GaN HEMTs," *IEEE Trans. Electron Devices*, vol. 67, no. 5, pp. 1924–1930, May 2020.

[11] B. Ubochi, S. Faramehr, K. Ahmeda, P. Igić, and K. Kalna, "Operational frequency degradation induced trapping in scaled GaN HEMTs," *Microelectron. Rel.*, vol. 71, pp. 35–40, Apr. 2017.

[12] M. Meneghini, A. Tajalli, P. Moens, A. Banerjee, E. Zanoni, and G. Meneghesso, "Trapping phenomena and degradation mechanisms in GaN-based power HEMTs," *Mater. Sci. Semicond. Process.*, vol. 78, pp. 118–126, May 2018.

[13] M. Gassoumi, M. M. Ben Salem, S. Saadaoui, B. Grimbert, J. Fontaine, C. Gaquiere, and H. Maaref, "The effects of gate length variation and trapping effects on the transient response of AlGaN/GaN HEMT's on SiC substrates," *Microelectron. Eng.*, vol. 88, no. 4, pp. 370–372, Apr. 2011.

[14] Y. Qin, B. Albano, J. Spencer, J. S. Lundh, B. Wang, C. Buttay, M. Tadjer, C. DiMarino, and Y. Zhang, "Thermal management and packaging of wide and ultra-wide bandgap power devices: A review and perspective," *J. Phys. D, Appl. Phys.*, vol. 56, no. 9, Mar. 2023, Art. no. 093001.

[15] S. Sharbati, I. Gharibshahian, T. Ebel, A. A. Orouji, and W.-T. Franke, "Analytical model for two-dimensional electron gas charge density in recessed-gate GaN high-electron-mobility transistors," *J. Electron. Mater.*, vol. 50, no. 7, pp. 3923–3929, Jul. 2021.

[16] S. S. S. Jaghargh and A. A. Orouji, "An AlGaN/GaN HEMT by the periodic pits in the buffer layer," *Phys. Scripta*, vol. 94, no. 10, Oct. 2019, Art. no. 105002.

[17] S. S. Sajjadi Jaghargh and A. A. Orouji, "An AlGaN/GaN HEMT by a reversed pyramidal channel layer: Investigation and fundamental physics," *Int. J. Numer. Model., Electron. Netw., Devices Fields*, vol. 33, no. 4, Jul. 2020, Art. no. e2719.

[18] T. R. Lenka and A. K. Panda, "Characteristics study of 2DEG transport properties of AlGaN/GaN and AlGaAs/GaAs-based HEMT," *Semiconductors*, vol. 45, no. 5, pp. 650–656, May 2011.

[19] M. J. Wang, B. Shen, F. J. Xu, Y. Wang, J. Xu, S. Huang, Z. J. Yang, K. Xu, and G. Y. Zhang, "High temperature dependence of the density of two-dimensional electron gas in $Al_{0.18}Ga_{0.82}N$/GaN heterostructures," *Appl. Phys. A, Solids Surf.*, vol. 88, no. 4, pp. 715–718, Jul. 2007.

[20] J. Li, M. Tang, and J. Mao, ''Analytical thermal model for AlGaN/GaN HEMTs using conformal mapping method,'' *IEEE Trans. Electron Devices*, vol. 69, no. 5, pp. 2313–2318, May 2022.

[21] M. A. Alim, A. Jarndal, C. Gaquiere, and G. Crupi, ''A study of DC and RF transconductance for different technologies of HEMT at low and high temperatures,'' *J. Mater. Sci., Mater. Electron.*, vol. 34, no. 10, p. 892, Apr. 2023.

[22] R. Mann, S. Rewari, S. Sharma, and R. S. Gupta, ''Dual gate AlGaN/GaN MOS-HEMT biosensor for electrical detection of biomolecules-analytical model,'' *Semicond. Sci. Technol.*, vol. 38, no. 3, Mar. 2023, Art. no. 035012.

[23] H. Luo, Z. Zhong, W. Hu, and Y. Guo, ''Analysis and modeling of the temperature-dependent nonlinearity of intrinsic capacitances in AlGaN/GaN HEMTs,'' *IEEE Microw. Wireless Compon. Lett.*, vol. 31, no. 4, pp. 373–376, Apr. 2021.

[24] M. S. Nazir, P. Kushwaha, A. Pampori, S. A. Ahsan, and Y. S. Chauhan, ''Electrical characterization and modeling of GaN HEMTs at cryogenic temperatures,'' *IEEE Trans. Electron Devices*, vol. 69, no. 11, pp. 6016–6022, Nov. 2022.

[25] N. Sahebghalam, M. Shalchian, A. Chalechale, and F. Jazaeri, ''High-temperature HEMT model,'' *IEEE Trans. Electron Devices*, vol. 69, no. 9, pp. 4821–4827, Sep. 2022.

[26] K. Ahmeda, B. Ubochi, B. Benbakhti, S. J. Duffy, A. Soltani, W. D. Zhang, and K. Kalna, ''Role of self-heating and polarization in AlGaN/GaN-based heterostructures,'' *IEEE Access*, vol. 5, pp. 20946–20952, 2017.

[27] B. Ubochi, K. Ahmeda, and K. Kalna, ''Buffer trap related knee walkout and the effects of self-heating in AlGaN/GaN HEMTs,'' *ECS J. Solid State Sci. Technol.*, vol. 6, no. 11, pp. S3005–S3009, 2017.

[28] D. Wilk, ''High-k gate dielectrics: Current status and materials properties condiderations,'' *J. Appl. Phys*, vol. 89, no. 10, pp. 5275–5423, 2001 2001.

[29] *ATLAS User's Manual*, I. J. S. C. Silvaco, Santa Clara, CA, USA, 2011, vol. 5.

[30] O. Ambacher, J. Smart, J. R. Shealy, N. G. Weimann, K. Chu, M. Murphy, W. J. Schaff, L. F. Eastman, R. Dimitrov, L. Wittmer, M. Stutzmann, W. Rieger, and J. Hilsenbeck, ''Two-dimensional electron gases induced by spontaneous and piezoelectric polarization charges in N- and ga-face AlGaN/GaN heterostructures,'' *J. Appl. Phys.*, vol. 85, no. 6, pp. 3222–3233, Mar. 1999.

[31] O. Ambacher, B. Foutz, J. Smart, J. R. Shealy, N. G. Weimann, K. Chu, M. Murphy, A. J. Sierakowski, W. J. Schaff, L. F. Eastman, R. Dimitrov, A. Mitchell, and M. Stutzmann, ''Two dimensional electron gases induced by spontaneous and piezoelectric polarization in undoped and doped AlGaN/GaN heterostructures,'' *J. Appl. Phys.*, vol. 87, no. 1, pp. 334–344, Jan. 2000.

[32] R. M. Chu, Y. G. Zhou, Y. D. Zheng, P. Han, B. Shen, and S. L. Gu, ''Influence of doping on the two-dimensional electron gas distribution in AlGaN/GaN heterostructure transistors,'' *Appl. Phys. Lett.*, vol. 79, no. 14, pp. 2270–2272, Oct. 2001.

[33] R. de Paiva, ''Theoretical study of the $Al_xGa_{1-x}N$ alloys,'' *Mater. Sci. Eng., B*, vol. 93, no. 1, pp. 2–5, May 2002.

[34] J. Kuzmik, ''Power electronics on InAlN/(In)GaN: Prospect for a record performance,'' *IEEE Electron Device Lett.*, vol. 22, no. 11, pp. 510–512, Nov. 2001.

[35] M. Li and Y. Wang, ''2-D analytical model for current–voltage characteristics and transconductance of AlGaN/GaN MODFETs,'' *IEEE Trans. Electron Devices*, vol. 55, no. 1, pp. 261–267, Jan. 2008.

[36] X. Cheng, M. Li, and Y. Wang, ''An analytical model for current–voltage characteristics of AlGaN/GaN HEMTs in presence of self-heating effect,'' *Solid-State Electron.*, vol. 54, no. 1, pp. 42–47, Jan. 2010.

[37] M. Gonschorek, J.-F. Carlin, E. Feltin, M. A. Py, and N. Grandjean, ''Self heating in AlInN/AlN/GaN high power devices: Origin and impact on contact breakdown and IV characteristics,'' *J. Appl. Phys.*, vol. 109, no. 6, Mar. 2011, Art. no. 063720.

[38] A. Pérez-Tomás, M. Placidi, N. Baron, S. Chenot, Y. Cordier, J. C. Moreno, A. Constant, P. Godignon, and J. Millán, ''GaN transistor characteristics at elevated temperatures,'' *J. Appl. Phys.*, vol. 106, no. 7, Oct. 2009, Art. no. 074519.

[39] A. Pérez-Tomás and A. Fontserè, ''AlGaN/GaN hybrid MOS-HEMT analytical mobility model,'' *Solid-State Electron.*, vol. 56, no. 1, pp. 201–206, Feb. 2011.

[40] J. Derluyn, ''Low leakage high breakdown e-mode GaN DHFET on Si by selective removal of in-situ grown Si_3N_4,'' in *IEDM Tech. Dig.*, Dec. 2009, pp. 1–4.

[41] B. L. Gelmont, M. Shur, and M. Stroscio, ''Polar optical-phonon scattering in three- and two-dimensional electron gases,'' *J. Appl. Phys.*, vol. 77, no. 2, pp. 657–660, Jan. 1995.

[42] M. K. Chattopadhyay and S. Tokekar, ''Temperature and polarization dependent polynomial based non-linear analytical model for gate capacitance of AlmGa1-mN/GaN MODFET,'' *Solid-State Electron.*, vol. 50, no. 2, pp. 220–227, Feb. 2006.

[43] Y. P. Varshni, ''Temperature dependence of the energy gap in semiconductors,'' *Physica*, vol. 34, no. 1, pp. 149–154, Jan. 1967.

[44] W. S. Yan, R. Zhang, X. Q. Xiu, Z. L. Xie, P. Han, R. L. Jiang, S. L. Gu, Y. Shi, and Y. D. Zheng, ''Temperature dependence of the pyroelectric coefficient and the spontaneous polarization of AlN,'' *Appl. Phys. Lett.*, vol. 90, no. 21, May 2007, Art. no. 212102.

[45] I. Vurgaftman, J. R. Meyer, and L. R. Ram-Mohan, ''Band parameters for III–V compound semiconductors and their alloys,'' *J. Appl. Phys.*, vol. 89, no. 11, pp. 5815–5875, Jun. 2001.

[46] V. Palankovski and R. Quay, *Analysis and Simulation of Heterostructure Devices*. Cham, Switzerland: Springer, 2004.

[47] D. M. Caughey and R. E. Thomas, ''Carrier mobilities in silicon empirically related to doping and field,'' *Proc. IEEE*, vol. 55, no. 12, pp. 2192–2193, Jan. 1967.

[48] M. A. K. Khan, M. A. Alim, and C. Gaquiere, ''2DEG transport properties over temperature for AlGaN/GaN HEMT and AlGaN/InGaN/GaN pHEMT,'' *Microelectronic Eng.*, vol. 238, Feb. 2021, Art. no. 111508.

[49] M. A. Alim, A. Z. Chowdhury, S. Islam, C. Gaquiere, and G. Crupi, ''Temperature-sensitivity of two microwave HEMT devices: AlGaAs/GaAs vs. AlGaN/GaN heterostructures,'' *Electronics*, vol. 10, no. 9, p. 1115, May 2021.

NAEEMUL ISLAM was born in Chittagong, Bangladesh, in 1994. He received the B.Sc. degree from the Department of Electrical and Electronic Engineering, International Islamic University Chittagong (IIUC), Bangladesh, in 2018. He is currently pursuing the M.Sc. degree with the School of Electrical and Electronic Engineering, Universiti Sains Malaysia (USM), Malaysia. He completed his bachelor's thesis on wave energy conversion system with Pelton turbine control strategies. He is also working on the characterization of the GaN HEMT power device by simulation. His main research interests include the simulation, design, fabrication and characterization of high RF and high-power devices on compound semiconductor materials, such as GaN HEMT.

MOHAMED FAUZI PACKEER MOHAMED received the B.Eng. degree (Hons.) in electrical and electronics engineering from Universiti Tenaga Nasional (UNITEN), Kajang, Selangor, Malaysia, in 2002, the M.Sc. degree in electronics system design engineering from Universiti Sains Malaysia (USM), Nibong Tebal, Pulau Pinang, in 2010, and the Ph.D. degree in electrical and electronics engineering from The University of Manchester (UoM), Manchester, U.K., in 2015.

In 2015, he joined the School of Electrical and Electronics Engineering, USM, as a Senior Lecturer. Prior to joining the university, he gained seven years of industrial experience, from 2002 to 2009, in semiconductor wafer fabrication and packaging. His current research interests include the simulation, design, fabrication, and characterization of high RF and high-power devices based on compound semiconductor materials. He is also keen on the research area of organic thin film transistors.

NORHAWATI AHMAD (Member, IEEE) received the B.Eng. degree (Hons.) in electrical and electronics engineering from Universiti Tenaga Nasional (UNITEN), Malaysia, in 2002, the master's degree in microelectronic engineering from Universiti Kebangsaan Malaysia (UKM), Malaysia, in 2005, and the Ph.D. degree in electrical and electronics engineering from The University of Manchester (UoM), U.K., in 2012. She started her academic career, in 2003, as a Lecturer with the Department of Electrical and Electronic Engineering, Universiti Teknologi MARA (UiTM). Since May 2004, she has been with the School of Microelectronic Engineering, Universiti Malaysia Perlis (UniMAP), Malaysia, formerly known as Kolej Universiti Kejuruteraan Utara Malaysia (KUKUM). Currently, she is an Associate Professor with the Faculty of Electronic Engineering and Technology, UniMAP. Her research involved high-speed pHEMT device modeling, RF and analog circuit designs, and measurement. She is also working with the GaN technology focusses on device modeling and circuit design.

MUAMMAR MOHAMAD ISA (Member, IEEE) is currently an Associate Professor with the Faculty of Electronic Engineering and Technology (fkten), Universiti Malaysia Perlis. With over 18 years of experience, he has held various leadership positions, including the Deputy Dean of Academic and Research and the Deputy Dean of the Center for Graduate Studies. He is a Registered Professional Technologist and actively contributes to curriculum development and quality assurance for undergraduate and postgraduate programs. His research interests include III-V devices, specializing in simulation, fabrication, and characterization for high-speed, high-frequency, and low-noise applications. He collaborates extensively with industries, particularly in developing the smart IoT systems for agricultural plantations. His expertise, dedication to excellence, and interdisciplinary approach make him a respected figure in the field of electronic engineering. His remarkable career leaves a lasting impact on both academia and industry, inspiring future engineers and technologists.

ALHAN FARHANAH ABD RAHIM received the B.Eng. degree (Hons.) in electronics engineering from the University of Southampton, U.K., in 1998, and the M.Sc. and Ph.D. degrees in solid state physics from Universiti Sains Malaysia, in 2003 and 2014, respectively. She is currently an Associate Professor with the Centre for Electrical Engineering Studies, Universiti Teknologi MARA, Cawangan Pulau Pinang, Malaysia. Her research interests include the synthesis and fabrication of semiconductor materials (group IV, III-V, porous semiconductors, and metal-oxides) through electrochemical, thermal evaporation, RF sputtering techniques for optoelectronic, and gas sensing applications. She is also keens on semiconductor modeling and simulation utilizing SILVACO TCAD for her research work.

KHALED AHMEDA received the B.Eng. degree in electrical and electronics engineering from the College of Petroleum Engineering, Al-Brega, Sirte University, Libya, in 2003, the M.Sc. degree in microelectronics from Universiti Kebangsaan Malaysia, Bangi, Malaysia, in 2005, and the Ph.D. degree in GaN HEMTs for power and RF applications. In 2006, he became an Assistant Lecturer with Sirte University. He was a Research Assistant with Swansea University, from 2017 to 2018, and a Research Visitor with the Nanoelectronic Devices Computational Group and the GaN Devices Modeling Group, Swansea University, from January 2018 to January 2020. He was an Associate Tutor with the Cardiff School of Technologies, Cardiff Metropolitan University, from January 2020 to July 2021. Currently, he is a Senior Device Engineer with Dynex Semiconductor Ltd. His current research interests include the modeling of III-nitrides-based devices, SiC MOSFET, reliability, and the characterization of GaN HEMTs.